Journal of Solid State Chemistry 184 (2011) 3080–3084

Contents lists available at SciVerse ScienceDirect

Journal of Solid State Chemistry

journal homepage: www.elsevier.com/locate/jssc

Synthesis, crystal structure and magnetic properties of the open framework compound $Co_3Te_2O_2(PO_4)_2(OH)_4$

Iwan Zimmermann [a,1], Reinhard K. Kremer [b,2], Mats Johnsson [a,*]

[a] Department of Materials and Environmental Chemistry, Stockholm University, SE-106 91 Stockholm, Sweden
[b] Max-Planck-Institut für Festkörperforschung, Heisenbergstrasse 1, D-70569 Stuttgart, Germany

ARTICLE INFO

Article history:
Received 18 June 2011
Received in revised form
12 September 2011
Accepted 18 September 2011
Available online 22 September 2011

Keywords:
Framework structure
Lone-pair element
Phosphate
Hydroxide
Antiferromagnetic

ABSTRACT

The new compound $Co_3Te_2O_2(PO_4)_2(OH)_4$ was synthesized using hydrothermal techniques. It crystallizes in the monoclinic space group $C2/m$ with the unit cell $a=19.4317(10)$ Å, $b=6.0249(3)$ Å, $c=4.7788(2)$ Å, $\beta=103.139(5)^\circ$. The crystal structure is an open framework having chains of edge sharing $[Co(1)O_6]$ octahedra. Other building blocks are $[TeO_3(OH)_2]$, $[PO_4]$ and $[Co(_2)O_2(OH)_4]$ connected mainly via corner sharing. The –OH groups protrude into channels in the structure. The magnetic susceptibility measured from 2 to 300 K shows two broad anomalies at around 21 K and 4 K, respectively. The peak at ~20 K is ascribed to a two-dimensional antiferromagnetic ordering of linear $[Co(1)O_6]$ chains coupled by interchain interaction via $[PO_4]$ groups in the Co(1) sheets. The second transition at 4 K is ascribed to a second antiferromagnetic ordering of the moments of the Co(2) entities via super–super exchange involving $[PO_4]$ and $[TeO_3(OH)_2]$ groups. This assignment is strongly supported by low-temperature heat capacity measurements indicating an entropy removal within the high-temperature transition of about twice the magnitude of the low-temperature transition.

1. Introduction

Cations of P-elements that have a stereochemically active nonbonded electron pair, *e.g.* Te^{4+}, Se^{4+}, and Sb^{3+}, often adopt an asymmetric or one-sided coordination. This fact makes the lone-pair electrons to help open up crystal structures. They thus enhance the possibility to form compounds exhibiting open framework structures [1,2] or layered compounds, where the layers are only weakly connected by van der Waals bonds and the lone-pairs protrude out from the layers [3,4]. The role of lone pair distortions in structural chemistry has been addressed by several researchers and is thought to result from a second-order Jahn–Teller (SOJT) distortion [5,6]. Utilizing lone-pair cations has proven to be highly successful in synthesizing new compounds with interesting physical properties. There are several examples of oxohalides containing e.g. Te^{4+} and late transition metal cations where the transition metal ions adopt low-dimensional arrangements such as two dimensional layers [4], one dimensional chains [7] or zero dimensional clusters [8,9]. The lone-pairs also enhance the possibility to form non-centrosymmetric compounds having non-linear optical properties [10,11]. Another interesting class of compounds are phosphates, which exhibit a rich structural chemistry, e.g. open framework structures [12,13]. There is a huge variety also in the physical properties such as electric, magnetic, and SHG properties to be expected when combining phosphate groups, lone-pair elements and transition metal cations [14,15].

Including lone-pair elements in phosphates allows for a new family of compounds having interesting properties. At present there are only a few compounds known within the Trm – Te – P – O (Trm=transition metal) system $A_2TeMo_2O_6(PO_4)_2$, A=K, Rb, Tl, Cs [16] and $BaMTeO_4(PO_4)$, M=Nb, Ta [17]. The structure and magnetic properties of the compound $Co_3Te_2O_2(PO_4)_2(OH)_4$ which we report here is to our best knowledge the first phase described containing Co^{2+}, Te^{4+} and phosphate groups. $Co_3Te_2O_2(PO_4)_2(OH)_4$ may be expected to exhibit interesting magnetic properties due to the arrangement of the Co^{2+} magnetic species in chains and in isolated atoms in between the chains.

2. Experimental

Single crystals of $Co_3Te_2O_2(PO_4)_2(OH)_4$ were prepared by hydrothermal synthesis from a mixture of 0.53 g (4 mmol) $CoCl_2$ (Sigma – Aldrich 97%), 0.43 g (2.7 mmol) TeO_2 (Sigma – Aldrich 99+%) and 0.30 g (2.6 mmol) $(NH_4)H_2PO_4$ (STREM chemicals 98+%) together with 10 ml deionized water in a 23 ml Teflon

* Corresponding author. Fax: +46 8 15 21 87.
E-mail addresses: iwan.zimmermann@mmk.su.se (I. Zimmermann), rekre@fkf.mpg.de (R.K. Kremer), mats.johnsson@mmk.su.se (M. Johnsson).
[1] Fax: +46 8 15 21 87.
[2] Fax: +49 711 689 1689.

0022-4596/$ - see front matter © 2011 Elsevier Inc. All rights reserved.
doi:10.1016/j.jssc.2011.09.023

lined steel autoclave heated to 180 °C for one week. Red block like crystals were separated manually from residual tellurium oxide for further analysis.

Single crystal X-ray diffraction experiments were carried out on an Oxford Diffraction Xcalibur3 diffractometer equipped with a graphite monochromator. The data collection was performed at 300 K using Mo$K\alpha$ radiation, $\lambda = 0.71073$ Å. Absorption correction and data reduction were done with the software CrysAlis RED that also was employed for the analytical absorption correction [18]. The structure solution was carried out with SIR92 [19] and the refinement with SHELXL [20] in the WINGX [21] environment. All atom positions were refined anisotropically. The hydrogen atoms could not be located by the X-ray diffraction experiment, but were added afterwards based on bond valence sum calculations. Crystal data are reported in Table 1. Atomic coordinates and isotropic temperature parameters for all atoms are given in the supplementary material. The structural drawings are made with the program DIAMOND [22].

The magnetic susceptibilities of a powder compact of $Co_3Te_2O_2(PO_4)_2(OH)_4$ have been measured under field-cooling and zero field-cooling conditions with a Physical Property Measurement System (PPMS) and a Magnetic Property Measurement System (MPMS) (both Quantum Design) at temperatures between 1.8 and 300 K in magnetic fields up to 7 T. The heat capacities of a small powder sample ($m = 2.5$ mg) was determined with a PPMS system equipped with a 3He cryostat employing the relaxation method.

Table 1
Crystal data and structure refinement parameters for $Co_3Te_2O_2(PO_4)_2(OH)_4$.

Empirical formula [a]	$Co_3Te_2O_2(PO_4)_2(OH)_4$
Formula weight (g/mol)	721.96
Temperature (K)	300
Wavelength (Å)	0.71073
Crystal system	Monoclinic
Space group	$C\,2/m$
a (Å)	19.4317(10)
b (Å)	6.0249(3)
c (Å)	4.7788(2)
α (deg)	90
β (deg)	103.139(5)
γ (deg)	90
Volume (Å^3)	544.83(5)
Z	2
Density$_{calc.}$ (g cm^{-3})	4.400
Absorption coefficient (mm^{-1})	10.141
F(0 0 0)	654
Crystal color	Red
Crystal habit	Block
Crystal size (mm^3)	0.0684 × 0.0389 × 0.0225
Theta range for data collection (deg)	4.13–32.08
Index ranges	$-26 \le h \le 28$ $-9 \le k \le 6$ $-7 \le l \le 7$
Reflections collected	3821
Independent reflections	978
Data/restraints/parameters	978/0/59
Goodness-of-fit on F^2	1.132
Final R indices [b] [$I > 2$sigma(I)]	$R_1 = 0.0354$ w$R_2 = 0.0919$
R indices (all data)	$R_1 = 0.0394$ w$R_2 = 0.0932$
Largest diff. peak and hole (eÅ^{-3})	2.632 and −1.844

[a] The refinement was done on the structure with the nominal formula $Co_3Te_2O_6(PO_4)_2$. The hydrogen atoms could not be detected by X-ray diffraction and were inserted in between O(5) and O(4) based on BVS calculations after the final refinement.

[b] $R_1 = \sum||F_o| - |F_c||/\sum|F_o|$; w$R_2 = \{\sum[w(F_o^2 - F_c^2)2]/\sum[w(F_o^2)^2]\}^{1/2}$.

3. Results and discussion

3.1. Crystal structure

The compound $Co_3Te_2O_2(PO_4)_2(OH)_4$ crystallizes in the monoclinic space group $C2/m$. An open framework structure is formed through the presence of the tellurium lone-pairs and the predominating corner sharing bonding character of the coordination polyhedra. A main feature of the crystal structure is that is has chains along [010] of edge sharing [Co(1)O_6] octahedra. Those chains are separated from each other by [$TeO_3(OH)_2$], [Co(2)$O_2(OH)_4$] and [PO_4] coordination polyhedra. The –OH groups protrude into channels running along [010], see Fig. 1.

The Te^{4+} ion is five coordinated by three oxygen and two hydroxide groups to form a distorted [$TeO_3(OH)_2$] square pyramid. Those tellurium coordination polyhedra do not polymerize which is otherwise common among tellurites [23]. The [$TeO_3(OH)_2$] groups involve three shorter Te–O bonds in the range 1.861(4)–1.994(3) Å and two longer bonds of 2.331(3) Å. The three shorter bonds to one O(3) and two O(5) build up a trigonal pyramid that is the most common coordination for Te^{4+}. Adding the two longer Te–O bonds a distorted square planar bipyramid is formed, see Figs. 2 and 3. This coordination is unusual for Te^{4+}, but has previously been observed [14,24–27]. The position of the hydroxide group is supported by bond valence sum (BVS) calculations, which have such a low value as 1.19 for O(5) when not including the hydrogen atom. Atom O(4) that bonds to Co(2) and P has a BVS of only 1.6 indicating that the hydrogen bond makes an additional contribution. The hydrogen atoms were put at a distance of 0.95 Å from O(5) pointing into the cavity in the structure towards O(4) and the resulting hydrogen bond length becomes 1.9 Å. The O(5)–H bonding distance was simply selected from BVS data to yield a total value of 2.0 for O(5). The resulting contribution of the hydrogen bond to O(4) then becomes 0.21

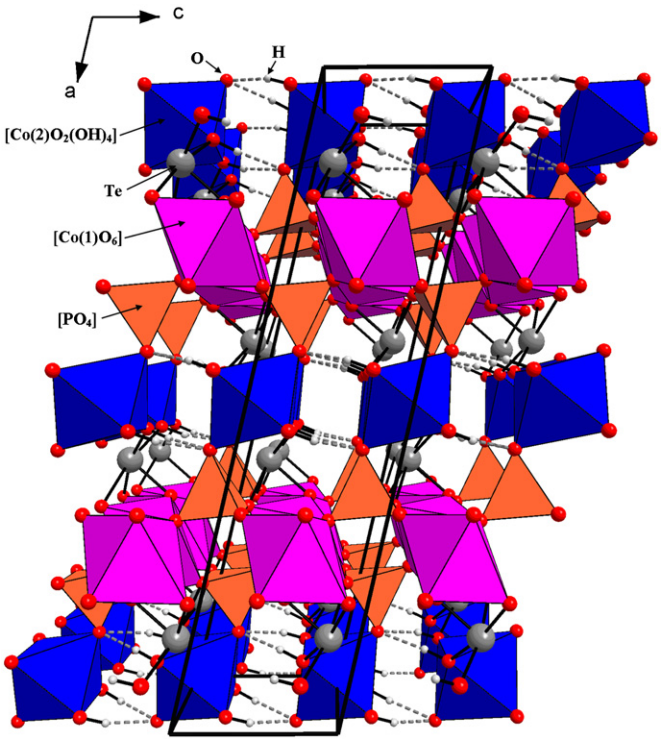

Fig. 1. Perspective view of the crystal structure of $Co_3Te_2O_2(PO_4)_2(OH)_4$ along [010]. The hydrogen bonds are displayed as dotted lines.

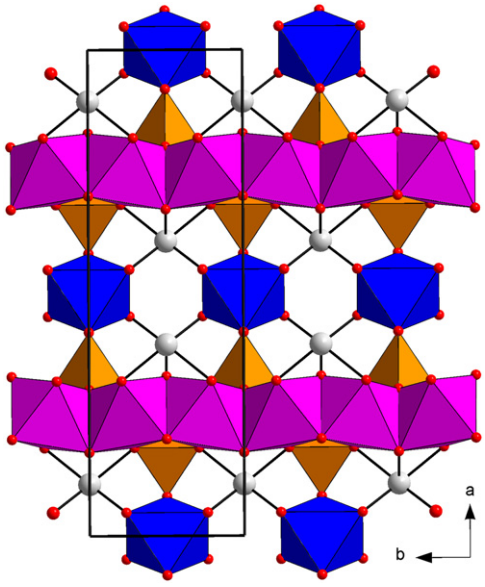

Fig. 2. Representation of the crystal packing along [001]. Hydrogen atoms are omitted for clarity. Same colors of the polyhedra and atoms as in Fig. 1.

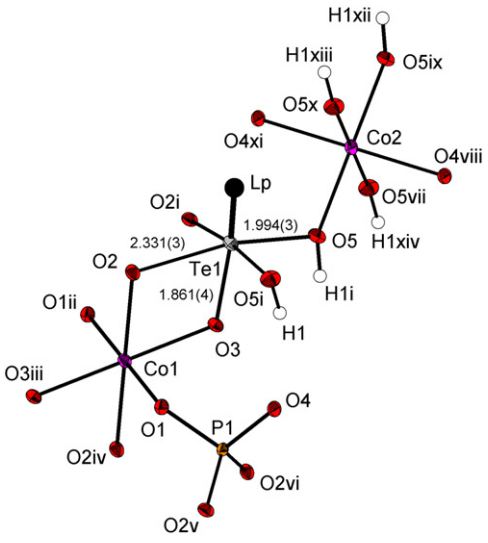

Fig. 3. Asymmetric unit plus selected symmetry equivalents of $Co_3Te_2O_2(PO_4)_2(OH)_4$. The black sphere represents the lone-pair electrons on Te^{4+}, the white circles represent the hydrogen atoms. Symmetry codes: (i) $x,-y+1,z$; (ii) $-x+0.5, y+0.5,-z+1$; (iii) $-x+0.5,y-0.5,-z+1$; (iv) $-x+0.5,-y+0.5,-z+1$; (v) $x,-y,z-1$; (vi) $x,y,z-1$; (vii) $x,-y+2,z$; (viii) $-x+1,y+1,-z+1$; (ix) $-x+1,-y+2, -z+2$; (x) $-x+1,y,-z+2$; (xi) x, $y+1$, $z+1$; (xii) $-x+1,y+1,-z+2$; (xiii) $-x+1, -y+1,-z+2$; (xiv) $x,y+1,z$.

resulting in a BVS value for O(4) of 2.0. Those distances are reasonable when compared with other similar compounds [28,29].

There are two crystallographically different cobalt atoms which both adopt distorted octahedral coordination geometries; $[Co(1)O_6]$ and $[Co(2)O_2(OH)_4]$. The Co–O bond lengths are in the range 2.051(3)–2.143(3) Å for Co(1) and 2.076(4)–2.147(3) Å for Co(2). The $[Co(1)O_6]$ octahedra are connected by edge sharing to form linear $[CoO_4]_\infty$ chains along [010]; the Co(1)–Co(1) distance within the chain is 3.012 Å. The angles between the cobalt atoms within the chain and the bridging oxygen atoms are 94.50(18)° for O(1) and 89.33(16)° for O(3) respectively. The $[Co(2)O_2(OH)_4]$ octahedron is not connected to other Co-polyhedra, but linked to phosphate and tellurate groups through corner sharing. The hydroxyl group is coordinated by both the Te and Co(2) atoms. To our knowledge this arrangement of a hydroxyl group bridging Te^{4+} and a transition metal ion has not been reported previously.

The phosphorous atom adopts a distorted tetrahedral coordination with bond lengths in the narrow range 1.530(4)–1.550(3) Å. The $[PO_4]$ tetrahedron is connected via corner sharing to the $[Co(1)O_6]$, $[Co(2)O_2(OH)_4]$ and the $[TeO_3(OH)_2]$ building blocks.

3.2. Magnetic properties

3.2.1. High temperature magnetic susceptibility

The low-field magnetic susceptibilities of $Co_3Te_2O_2(PO_4)_2(OH)_4$ measured in a field of 0.1 T are shown in Fig. 4. Field and zero field cooled curves were found to be nearly identical. The susceptibility shows a maximum at ~20 K followed by a rapid decrease due to antiferromagnetic coupling most likely due to ordering of the Co(1) ions within the linear chains. At around 5 K an additional maxima with lower intensity is observed, which is more difficult to link to the structure and could be due to super–super exchange involving the Co(2) ions. The inverse susceptibility curve slightly bends above 20 K due to critical fluctuations. Above ~40 K a linear behavior is observed. A least-squares fit to the Curie–Weiss law: $\chi = C/(T-\theta)+\chi_0$ between 40 and 330 K gives $\theta = -10.3(5)$ K and $C = 10.42(4)\,cm^3\,K\,mol^{-1}$ and $\chi_0 = 5(2)\times10^{-5}\,cm^3\,mol^{-1}$. The negative Curie–Weiss temperature θ indicates predominant antiferromagnetic spin-exchange interaction; χ_0 comprising temperature independent diamagnetic contributions from the electrons in closed shells ($-76\times10^{-6}\,cm^3\,mol^{-1}$, as calculated from Selwood's increments) and temperature independent van Vleck contributions, which for Co^{2+} are of the order of $\sim100\times10^{-6}\,cm^3\,mol^{-1}$, consistent with our experimental findings [30,31].

From the effective magnetic moment μ_{eff} by using Eq. (1)

$$\mu_{eff} = \sqrt{3k_B/xN_A\mu_B}\sqrt{C} \quad (1)$$

where $x=3$ is the number of Co atoms in the chemical formula, one obtains an effective magnetic moment $\mu_{eff}=5.27(1)\ \mu_B$ per metal ion. Typical values of μ_{eff} observed for Co^{2+} in octahedral systems due to orbital contributions are in the range 4.3–5.2 μ_B, that is consistent with our experimental observation [32,33].

3.2.2. Low temperature magnetic ordering

The magnetic susceptibility measurements indicate long-range antiferromagnetic ordering at low temperatures as proposed by the peak and the rapid decrease of the susceptibility below (see Fig. 5d). At low temperatures an additional shallow hump appears

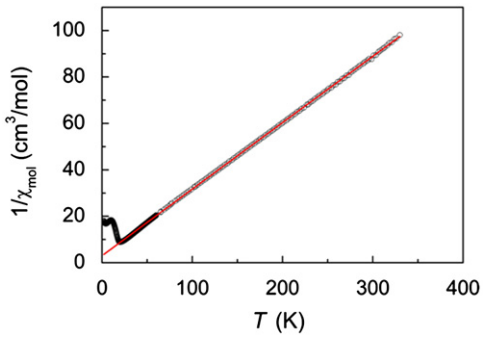

Fig. 4. Magnetic susceptibility of $Co_3Te_2O_2(PO_4)_2(OH)_4$ measured with a field of 0.1 T. Antiferromagnetic ordering takes place at 21 K. At around 5 K an additional maxima with lower intensity is observed, see text. The inverse susceptibility curve above $T_N=21$ K is slightly bended. A fit to the Curie–Weiss law in the range 40–300 K gives $\theta=-10.3(5)$ K and $C=10.42(4)\ cm^3\,K\,mol^{-1}$ and $\chi_0=5(2)\times10^{-5}\,cm^3\,mol^{-1}$ (solid red line). (For interpretation of the references to color in this figure legend, the reader is referred to the web version of this article.)

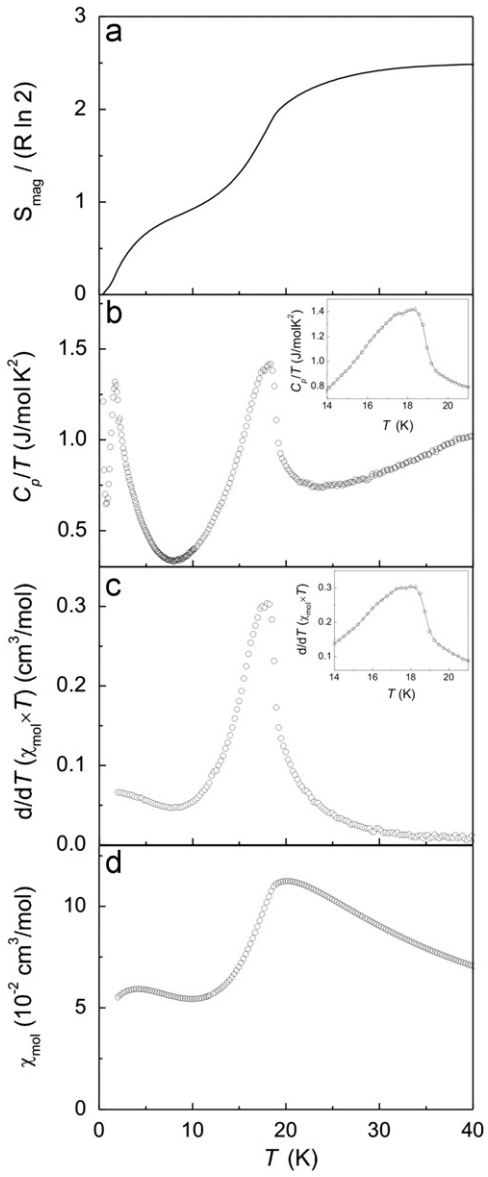

Fig. 5. Low-temperature magnetic susceptibility (0.1 T) and heat capacity, *Cp*/T, of $Co_3Te_2O_2(PO_4)_2(OH)_4$ (panels (d) and (b), respectively). The panels (a) and (c) show the magnetic entropy versus temperature and Fisher's heat capacity. The insets display the peaks in an enlarged scale.

which is associated to ordering of the Co(2) cations. The heat capacity (Fig. 5b) and the quantity $d/dT(\chi_{mol}\times T)$ (Fisher's heat capacity [34]), see Fig. 5c, exhibit anomalies of similar shape centered at identical temperatures indicating long-range antiferromagnetic ordering to occur below 17.7(3) K. A closer inspection reveals a splitting of both peaks by about 0.7 K (see insets in Fig. 5b and c). The quantity C_p/T displayed in Fig. 5c reveals an additional sharp peak at ~1.5 K indicating additional entropy removal also at very low temperatures.

The magnetic contribution to the heat capacity (not shown in Fig. 5) was obtained by subtracting a lattice contribution to the heat capacity. The latter was estimated by fitting an even polynomial, $C_{lat}/T=\sum_{n=1}^{6} a_{2n}T^{2n}$, to the high-temperature data ($T>40$ K) and extrapolating to $T\rightarrow 0$ K. Subsequently the magnetic entropy $S_{mag}(T)$ was obtained by integrating $C_{mag}(T)/T$. The magnetic entropy is removed in two consecutive steps centered at about 17 K and 2 K, reflecting the magnetic anomalies found in the heat capacity. At 40 K the magnetic entropy assumes a value of about 2.5 R ln 2. For an effective $S=1/2$ system as it is given with Co^{2+} in a distorted octahedral environment one expects the magnetic entropy per Co atom, $S_{mag}(T)$, to approach an entropy value of *R*ely 2 for as $T\rightarrow\infty$, where *R* is the molar gas constant. Inspection of Fig. 5 (a) reveals that the entropy at 40 K falls short of this value by about 15%. This deficiency may be due to a partly inadequate construction of the lattice heat capacity leading to underestimating C_{mag}. Unaffected by this discrepancy is the ratio of the two steps which is close to 1:2, indicating long-range ordering of two Co moments in a first step at 17.7 K, which obviously can be attributed to the two Co(1) atoms in the corrugated chains. Spin exchange coupling of these chain Co atoms to the Co(2) moments and between the Co(2) moments in crystallographic positions between the chains is smaller and consequently these moments order at a significantly lower temperature. This scenario allows understanding the two separated steps in the magnetic entropy and also explaining the weak susceptibility anomaly seen at low temperatures. The splitting of the heat capacity anomaly associated to the antiferromagnetic ordering at 17.7 K remains unexplained at present. Owing to the large uniaxial anisotropy of the Co moments a strong magnetoelastic coupling and a magnetostructural phase transition might be the origin of this splitting.

3.2.3. *Spin-flop transition at high magnetic fields and low temperature*

Finally we briefly describe the magnetic behavior of $Co_3Te_2O_2(PO_4)_2(OH)_4$ at higher magnetic fields. We have observed that the decrease of the magnetic susceptibility below 17.7 K disappears in field above ~3 T. A magnetization measurement carried out at 2 K indeed reveals a non-hysteretic spin-flop like transition at 2.72(3) T with a change from a linear field dependency of the magnetization to a saturation-type characteristic superposed on a linear increasing magnetization, see Fig. 6. By extrapolating the linear field dependence to high field and subtracting it from the magnetization, a saturation moment of ~1.5 μ_{Bohr} per 3 Co atoms results. Spin exchange coupling between the Co(1) moments appears to be much larger and can only be aligned by substantially higher fields. At lower fields in which our magnetization measurements were carried out they merely contribute to the linear background.

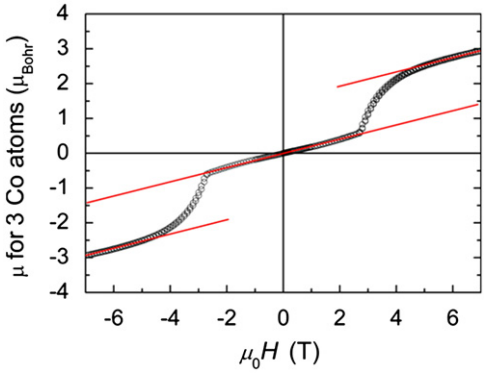

Fig. 6. Magnetic moment (per 3 Co atoms) of a polycrystalline compact sample of $Co_3Te_2O_2(PO_4)_2(OH)_4$ determined at 2 K. The red straight lines extrapolate the linear field dependence of the magnetization observed for small fields to magnetic fields above (below) the spin flop transition. (For interpretation of the references to color in this figure legend, the reader is referred to the web version of this article.)

4. Summary and Conclusions

The new compound $Co_3Te_2O_2(PO_4)_2(OH)_4$ has been obtained by hydrothermal synthesis. It crystallizes in the monoclinic space group $C2/m$. and to our best knowledge it is the first compound containing all of Te^{4+}, Co^{2+} and P^{5+}.

The dominating corner sharing of the coordination polyhedra and the stereochemically active lone-pair electrons on Te^{4+} are responsible for the open framework structure. There are two crystallographic different Co^{2+} ions having different coordination polyhedra: $[Co(1)O_6]$ octahedra that form chains along [010] by edge sharing and $[Co(2)O_2(OH)_4]$ that are surrounded by $[TeO_3(OH)_2]$, and $[PO_4]$ coordination polyhedra. The hydrogen atoms could not be directly detected by X-ray diffraction, but bond valence calculations confirmed, that it is O(5) that has a covalent bond to H. This hydrogen atom also contribute to BVS for O(4) via hydrogen bonding. The oxygen–hydrogen distances were calculated by assuming that BVS should be 2.0 for both O(5) and O(4). The contribution by H then was 0.8 to O(5) and 0.2 to O(4) that corresponds to a distance of O(5)–H that is 0.95 Å and a O(4) –H distance that is 1.9 Å.

The interpretation of the magnetic properties of $Co_3Te_2O_2(PO_4)_2(OH)_4$ has to consider the arrangement of the Co(1) in linear chains which via PO_4 polyhedra are connected into sheets. Isolated $Co(2)O_6$ polyhedra are located in-between the Co(1) sheets and connect to these via $[PO_4]$ and $[TeO_3(OH)_2]$ polyhedra. Because of spin–orbit interaction Co^{2+} in an octahedral crystal field exhibits an effective $S=1/2$ ground state the g-factor of which typically shows large anisotropy as the octahedral environment is distorted and the symmetry of the crystal field is lowered. Therefore, exchange coupling between Co^{2+} is very often well described by an Ising-type exchange interaction (see e.g. Ref. [34]).

With deceasing temperature the chains undergo short range antiferromagnetic ordering and due to interchain coupling to neighboring chains two-dimensional antiferromagnetic ordering in the Co(1) sheets takes place. Two-dimensional Ising systems undergoing long-range ordering gives rise to a sharp anomaly in the specific heat even in case of a large difference of intrachain and interchain exchange coupling [35,36]. The shape of the susceptibility peak as well as the sharp heat capacity anomaly being similar to the anomalies found in Fisher's heat capacity are consistent with this assignment.

The magnetic susceptibility shows a maximum at $\sim$20 K, which does not exhibit the typically round shape expected for one-dimensional magnetic systems with short range antiferromagnetic correlations (see e.g. [33,37]) but can be explained by two-dimensional antiferromagnetic ordering of the Co(1) linear chains due to interchain coupling in the Co(1) sheets (see e.g. examples in [38]).

Exchange coupling between the Co(1) and the Co(2) and between the Co(2) moments themselves is much weaker and long range ordering takes place at much lower temperatures and gives rise to the anomalies in the heat capacity and the magnetic susceptibility at about 2 K. The entropy proves a clear ratio of 2:1 associated with the ordering of the Co(1) and the Co(2) moments, respectively, strongly supporting our scenario of subsequent long range ordering of the Co(1) moments first succeeded by the Co(2) moments at lower temperature. A spin flop transition with subsequent saturation above the flop field is observed and attributed to saturation of the Co(2) moments.

The negative Weiss temperature $\theta=-10.3$ K indicates predominant overall antiferromagnetic interaction. The effective magnetic moment is $\mu_{eff}=5.27\ \mu_B$ per metal ion. The analysis of the magnetic entropy indicates strong spin-exchange coupling within the Co(1) chains while the coupling to the intermediate Co(2) atoms and coupling between them is significantly smaller. Consequently, the Co(2) moments can be easily aligned with a moderate external magnetic field.

Acknowledgment

This work has in part been carried out through financial support from the Swedish Research Council.

Appendix A. Supporting information

Supplementary data associated with this article can be found in the online version at doi:10.1016/j.jssc.2011.09.023.

References

[1] K.M. Ok, P.S. Halasyamani, Inorg. Chem. 41 (2002) 3805–3807.
[3] R. Becker, M. Johnsson, R.K. Kremer, P. Lemmens, J. Solid State Chem. 178 (2005) 2024–2029.
[2] D. Zhang, M. Johnsson, R.K. Kremer, D. Wulferding, P. Lemmens, Inorg. Chem. 48 (2009) 6599–6603.
[4] R. Becker, M. Prester, H. Berger, M. Johnsson, D. Drobac, I. Zivkovic, Solid State Sciences. 9 (2007) 223–230.
[5] R.G. Pearson, J. Am. Chem. Soc. 91 (1969) 4947–4955.
[6] U.V. Waghmare, N.A. Spaldin, H.C. Kandpal, R. Seshadri, Phys. Rev. B 67 (2003) 125111.
[7] R. Fredrickson-Takagi, D. Torino-Hjelmqvist, M. Johnsson, S. Lidin, Solid State Sci. 11 (2009) 13–17.
[8] R. Takagi, M. Johnsson, V. Gnezdilov, R.K. Kremer, W. Brenig, P. Lemmens, Phys. Rev. B 74 (2006) 014413-1–014413-8.
[9] R. Becker, M. Johnsson, R.K. Kremer, H.-H. Klauss, P. Lemmens, J. Am. Chem. Soc. 128 (2006) 15469–15475.
[10] P.S. Halasyamani, K.R. Poppelmeier, Chem. Mater. 10 (1998) 2753–2769.
[11] P.S. Halasyamani, Chem. Mater. 16 (2004) 3586–3592.
[12] L.-Q. Fan, J.-H. Wu, Y.F. Huang, Z. Anorg. Allg. Chem. 634 (2008) 534–538.
[13] R.-K. Chiang, C.-C. Huang, C.-R. Lin, C.-S. Wur, J. Solid State Chem. 156 (2001) 242–246.
[14] M.K. Kim, S.H. Kim, H.-Y. Chang, P.S. Halasyamani, K.M. Ok, Inorg. Chem. 49 (2010) 7028–7034.
[15] N.F. Kharchenko, V.M. Khrustalev, V.N. Savitskii, Low Temperature Phys. 36 (2010) 558–564.
[16] A. Guesdon, B. Raveau, Chem. Mater. 12 (2000) 2239–2243.
[17] K.M. Ok, J. Orzechwski, P.S. Halasyamani, Inorg. Chem. 43 (2004) 964–968.
[18] Oxford diffraction, CrysAlisCCD and CrysAlisRED, Oxford Diffraction Ltd., Abingdon, Oxfordshire, England, 2006.
[19] A. Altomare, G. Cascarano, C. Giacovazzo, A. Guagliardi, M.C. Burla, G. Polidori, M. Camalli, J. Appl. Cryst. 27 (1994) 435.
[20] G.M. Sheldrick, Acta Crystallogr. A: Found. Crystallogr A64 (2008) 112.
[21] L.J. Farrugia, J. Appl. Crystallogr. 32 (1999) 837.
[22] G. Bergerhoff, 1996, DIAMOND, Bonn, Germany.
[23] J.-G. Mao, H.-L. Jiang, F. Kong, Inorg. Chem. 47 (2008) 8498–8510.
[24] H. Mayer, M. Weil, Z. Anorg. Allg. Chem. 629 (2003) 1068–1072.
[25] K. Jung, H. Kim, H. Yun, J. Do, Z. Anorg. Allg. Chem. 632 (2006) 1582–1585.
[26] K.M. Ok, P.S. Halasyamani, J. Solid State Chem. 179 (2006) 1345–1350.
[27] J.-H. Kim, P.S. Halasyamani, J. Solid State Chem. 181 (2008) 2108–2112.
[28] J.C. Jumas, M. Maurin, E. Philippot, J. Fluorine Chem. 8 (1976) 329–340.
[29] C.R. Feger, J.W. Kolis, K. Gorny, C. Pennington, J. Solid State Chem. 143 (1999) 254–259.
[30] P.W. Selwood, Magnetochemistry, 2nd ed., Interscience, New York, 1956.
[31] H. Lueken, Magnetochemie, Teubner, Leipzig, 1999.
[32] U. Müller, Inorganic Structural Chemistry, John Wiley & Sons, New York, 2007, p. 235.
[33] R.L. Carlin, Magnetochemistry, Springer, Heidelberg, 1986.
[34] M.E. Fisher, Philos. Mag. 7 (1962) 1731–1743.
[35] L. Onsager, Phys. Rev. 65 (1944) 117–149.
[36] see e.g. D.C. Mattis, The Theory of Magnetism II, Springer, Heidelberg, 1985 p. 89ff.
[37] D.C. Johnston, R.K. Kremer, M. Troyer, X. Wang, A. Klümper, S.L. Budko, A.F. Panchula, P. Canfield, Phys. Rev. B 61 (2000) 9558–9606.
[38] L.J. deJongh, A.R. Miedema, Adv. Phys. 50 (2001) 947–1170.